Intraocular Pressure Elevation Induces Mitochondrial Fission and Triggers OPA1 Release in Glaucomatous Optic Nerve

Won-Kyu Ju,[1,2] *Keun-Young Kim,*[3] *James D. Lindsey,*[1,2] *Mila Angert,*[1,2] *Karen X. Duong-Polk,*[1,2] *Ray T. Scott,*[3] *James Jaeyoung Kim,*[3] *Ismail Kukhmazov,*[3] *Mark H. Ellisman,*[3] *Guy A. Perkins,*[3] *and Robert N. Weinreb*[1,2]

Purpose. To determine whether elevation of intraocular pressure (IOP) triggers mitochondrial fission and ultrastructural changes and alters optic atrophy type 1 (OPA1) expression and distribution in the optic nerve (ON) of glaucomatous DBA/2J mice.

Methods. IOP in the eyes of DBA/2J mice was measured, and mitochondrial structural changes were assessed by conventional electron microscopy (EM) and EM tomography. Cytochrome *c* oxidase IV subunit 1 (COX), OPA1, and Dnm1, a rat homologue of dynamin-related protein-1, mRNA were measured by quantitative (q)PCR. COX and OPA1 protein distribution was assessed by immunocytochemistry and Western blot.

Results. Excavation of the optic nerve head (ONH), axon loss, and COX reduction were evident in 10-month-old glaucomatous ONHs of eyes with >20 mm Hg IOP elevation. EM analysis showed mitochondrial fission, matrix swelling, substantially reduced cristae volume, and abnormal cristae depletion in 10-month-old glaucomatous ONH axons. The mean length of mitochondrial cross section in these axons decreased from 858.2 ± 515.3 nm in 3-month-old mice to 583.3 ± 298.6 nm in 10-month-old glaucomatous mice ($P < 0.001$). Moderate reductions of COX mRNA were observed in the 10-month-old DBA/2J mice's ONHs. Larger reductions of OPA1 immunoreactivity and gene expression were coupled with larger increases of Dnm1 gene expression in 10-month-old glaucomatous ONH. Subcellular fractionation analysis indicates increased release of both OPA1 and cytochrome *c* from mitochondria in 10-month-old glaucomatous ONs.

Conclusions. IOP elevation may directly damage mitochondria in the ONH axons by promoting reduction of COX, mitochondrial fission and cristae depletion, alterations of OPA1 and Dnm1 expression, and induction of OPA1 release. Thus, interventions to preserve mitochondria may be useful for protecting against ON degeneration in glaucoma. (*Invest Ophthalmol Vis Sci.* 2008;49:4903–4911) DOI:10.1167/iovs.07-1661

Elevated intraocular pressure (IOP) is an important risk factor for optic nerve damage in glaucoma.[1] However, the precise pathophysiological relationships among elevated IOP, glaucomatous optic nerve (ON) damage, and retinal ganglion cell (RGC) death are poorly understood. Mitochondrial changes have been identified in association with neuronal death in other models of central nervous system disease.[2,3] In addition, there is evidence of abnormal mitochondrial respiration in patients with glaucoma.[4] Recently, we found that moderately elevated hydrostatic pressure can induce abnormal cristae depletion, cytochrome *c* release, cellular ATP reduction, and translocation of dynamin-related protein 1 (Drp-1) in differentiated RGC-5 cells.[5] Further, we found that elevated hydrostatic pressure triggers release of optic atrophy type 1 protein (OPA1) and cytochrome *c* and induces subsequent apoptotic cell death in differentiated RGC-5 cells (Ju WK, et al. *IOVS* 2007;48:ARVO E-Abstract 5551). These observations raise the possibility that pressure-induced mitochondrial dysfunction contributes to RGC death and ON degeneration in glaucoma.

In healthy cells, mitochondria are autonomous and morphologically dynamic organelles that structurally reflect a precise balance of ongoing fission and fusion within a cell.[6–8] This balance is regulated by a family of dynamin-related GTPases that exert opposing effects. OPA1, the human orthologue of Mgm1p/Msp1p, and the mitofusins are required for mitochondria fusion. Dynamin-related protein-1 (Drp-1) regulates mitochondrial fission.[7–9] Mutations in OPA1, a dynamin-related GTPase that is involved in various processes related to mitochondrial inner membrane structural dynamics, are linked with neurodegenerative disease in humans and cause autosomal dominant optic atrophy (ADOA), the most common form of hereditary optic neuropathy.[10,11]

OPA1 is expressed in the soma and axons of RGCs and horizontal cells.[12–15] However, the specific functional roles of OPA1 in these cells remain unknown. Emerging evidence suggests that downregulation of OPA1 causes mitochondrial fission, leading to cytochrome *c* release and apoptosis in HeLa cells, and induces aggregation of the mitochondrial network in purified RGCs.[16–19] Proteolytic processing of OPA1 has been observed during mitochondrial fission, although its significance is unclear.[20–23] Also, OPA1 release during mitochondrial fission contributes to apoptotic cell death.[18,22] Nevertheless, it is unknown whether IOP elevation can alter OPA1 expression and distribution in the ON degeneration of glaucoma.

To investigate these questions in an in vivo model of glaucoma, we evaluated whether IOP elevation triggers mitochondrial fission and ultrastructural changes and alters OPA1 expression and distribution in the ON of DBA/2J mice, an extensively characterized strain that spontaneously develops elevated IOP.[24–32]

From the [1]Hamilton Glaucoma Center, the [2]Department of Ophthalmology, and the [3]National Center for Microscopy and Imaging Research, School of Medicine, University of California San Diego, La Jolla, California.

Supported by National Eye Institute Grants EY01466 (JDL) and EY105990 (RNW) and National Center for Research Resources (NCRR) Grant P41 RR004050 (MHE).

Submitted for publication December 27, 2007; revised March 31, 2008; accepted September 5, 2008.

Disclosure: **W.-K. Ju**, None; **K.-Y. Kim**, None; **J.D. Lindsey**, None; **M. Angert**, None; **K.X. Duong-Polk**, None; **R.T. Scott**, None; **J.J. Kim**, None; **I. Kukhmazov**, None; **M.H. Ellisman**, None; **G.A. Perkins**, None; **R.N. Weinreb**, None

The publication costs of this article were defrayed in part by page charge payment. This article must therefore be marked "*advertisement*" in accordance with 18 U.S.C. §1734 solely to indicate this fact.

Corresponding author: Won-Kyu Ju, Hamilton Glaucoma Center and Department of Ophthalmology, University of California San Diego, La Jolla, CA 92037-0946; danielju@glaucoma.ucsd.edu.

Materials and Methods

Chemicals

All chemicals were from Sigma-Aldrich (St. Louis, MO) unless otherwise noted.

Animals

All procedures concerning animals were in accordance with the ARVO Statement for the use of Animals in Ophthalmic and Vision Research. Adult 3-, 6-, 7- to–8-, 9- to 10-, and 12-month-old female DBA/2J mice (The Jackson Laboratory, Bar Harbor, ME) and 3-, 6-, and 10-month-old female C57BL/6 mice (Harlan Sprague-Dawley, Inc., Indianapolis, IN) were housed in covered cages, fed with a standard rodent diet ad libitum, and kept on a12-hour light–12-hour dark cycle.

IOP Measurement

IOP measurement was performed as described previously.[24,33] Each of the 10- and 12-month-old DBA/2J mice used in this study had a single IOP measurement per month starting at 6 months of age (to confirm development of spontaneous IOP elevation exceeding 20 mm Hg). The glaucomatous DBA/2J mice that have confirmed IOP elevation were obtained in 65.3% (64/98) at 10 months of age. Also, each of the 3-, 6-, and 10-month-old nonglaucomatous C57BL/6 mice used in this study had a single IOP measurement. After anesthesia with a mixture of ketamine (100 mg/kg, Ketaset; Fort Dodge Animal Health, Fort Dodge, IA) and xylazine (9 mg/kg, TranquiVed; Vedeco, Inc., St. Joseph, MO), a sterilized, water-filled microneedle with an external diameter of 50 to 70 μm was used to cannulate the anterior chamber. The microneedle was then repositioned to minimize corneal deformation and to ensure that the eye remained in its normal position. The microneedle was connected to a pressure transducer (Blood Pressure Transducer; WPI, Sarasota, FL), which relayed its signal to a bridge amplifier (Quad Bridge; AD Instruments [ADI], Castle Hill, NSW, Australia). The amplifier was connected to an analogue-to-digital converter (Power Laboratory; ADI) and a computer (G4 Macintosh; Apple Computer Inc., Cupertino, CA).

Tissue Preparation

Light-adapted mice were anesthetized with isoflurane and killed by IP injection of ketamine and xylazine. The ONs were dissected from the choroid and fixed with 4% paraformaldehyde in 0.1 M phosphate buffer (PB, pH 7.4) for 2 hours at 4°C. After several washes in PB, the ONs were dehydrated through graded ethanols and then embedded in a polyester wax, as described previously.[14] For Western blot analyses, whole ONs were immediately used or frozen in liquid nitrogen and stored at −70°C until used.

Immunohistochemical Analyses

Immunohistochemical staining of 7-μm wax sections of full-thickness ON was performed with the immunofluorescent method as previously described.[14] Five sections per wax block from each age group (n = 3 mice/group) were used for immunohistochemical analysis. Primary antibodies were mouse monoclonal antibody against COX (1:500; Invitrogen-Molecular Probes, Eugene, OR) and polyclonal rabbit anti-mOPA1 antibody (1:1000, a gift of Takumi Misaka, The University of Tokyo, and Yoshihiro Kubo, National Institute for Physiological Sciences, Japan).[34] Polyclonal rabbit anti-mOPA1 antibody was directed against amino acids 938-960 of mouse OPA1 protein was generated and peptide affinity purified as previously described.[14,34] To prevent nonspecific background, tissues were incubated with 1% bovine serum albumin/PBS for 1 hour at room temperature and then with the primary antibody against COX or OPA1 for 16 hours at 4°C. After several wash steps, the tissue was incubated with the secondary antibodies, peroxidase-conjugated goat anti-mouse IgG or goat anti-rabbit IgG (1:100, Invitrogen-Molecular Probes) for 4 hours at 4°C and then washed with PBS. The sections were counterstained with a nucleic acid stain (Hoechst 33342 1 μg/mL; Invitrogen-Molecular Probes) in PBS.

Images were captured under fluorescence microscopy (Eclipse microscope, model E800; Nikon Instruments Inc., Melville, NY) equipped with a digital camera (SPOT; Diagnostic Instrument, Sterling Heights, MI). Image exposures were the same for all tissue sections and were acquired with commercial software (Simple PCI ver. 6.0 software; Compix Inc., Cranberry Township, PA).

Electron Microscopy

For conventional electron microscopy (EM), two eyes from each group (n = 2 mice) were fixed via cardiac perfusion with solution at 37°C in 2% paraformaldehyde, 2.5% glutaraldehyde (Ted Pella, Redding, CA) in 0.15 M sodium cacodylate (pH 7.4) and placed in precooled fixative on ice for 1 hour. The following procedure was used to optimize mitochondrial structural preservation and membrane contrast.[5,35,36] The ONHs were dissected with 0.15 M sodium cacodylate plus 3 mM calcium chloride (pH 7.4) on ice and then postfixed with 1% osmium tetroxide, 0.8% potassium ferrocyanide, 3 mM calcium chloride in 0.1 M sodium cacodylate (pH 7.4) for 1 hour, washed with ice-cold distilled water, poststained with 2% uranyl acetate at 4°C, dehydrated through graded ethanols, and embedded in resin (Durcupan; Fluka, St. Louis, MO). Ultrathin (70 nm) sections were poststained with uranyl acetate and lead salts before imaging (1200FX transmission EM operated at 80 kV; JEOL, Tokyo, Japan). The negatives were digitized at 1800 dpi (CoolScan; Nikon) system, giving an image size of 4033 × 6010 pixel array and a pixel resolution of 1.77 nm.[37–39] The lengths of mitochondrial cross sections at the longest extent were measured in the unmyelinated ONH, as described previously.[5] For unbiased sampling, all the mitochondria in an image were measured.

A power analysis was conducted on the measured mean mitochondrial lengths using the tool found at http://www.power-analysis.com/. A sampling size of about 1000 each for the 3- and 10-month-old conditions was chosen to anticipate the likelihood that the study would yield a significant effect and to minimize both type I and type II error rates.

Electron Microscope Tomography

Sections of prelaminar unmyelinated ONH axons from each group were cut at thicknesses of 400 to 500 nm. Sections were then stained 30 minutes in 2% aqueous uranyl acetate, followed by 15 minutes in lead salts. Fiducial cues consisting of 15 nm colloidal gold particles were deposited on opposite sides of the section. For each reconstruction, a series of images at regular tilt increments was collected with an intermediate-voltage electron microscope operated at 400 kV (model 4000EX; JEOL). Before a tilt series was initiated, the specimens were irradiated to reduce anisotropic specimen thinning during image collection. Tilt series were recorded on film at 20,000 magnification with an angular increment of 2° from −60° to +60° about an axis perpendicular to the optical axis of the microscope using a computer-controlled goniometer to increment the angular steps accurately. The illumination was held to near parallel beam conditions and optical density was maintained constant by varying the exposure time. The negatives were digitized at 1800 dpi (CoolScan; Nikon), producing images of size 4033 × 6010 pixels. The pixel resolution was 0.7 nm. The IMOD package was used for rough alignment (http://bio3d.colorado.edu/imod/ provided in the public domain by the Boulder Laboratory for 3-Dimensional Electron Microscopy of Cells and the Regents of the University of Colorado, Boulder, CO). Briefly, we tracked fiducial gold particles across all images of the tilt series that had been roughly aligned by cross-correlation.[40] Fine alignment and volume reconstruction were performed with the TxBR package.[41] This software removes image distortions by generating a global nonlinear model of electron trajectories and then back-projecting along these trajectories to build up the volume. Volume segmentation was performed by manual tracing in the planes of highest resolution with the program Xvoxtrace (www.ncmir.ucsd.edu/downloads/xvoxtrace/ provided in the public domain by the National Center for Microscopy and Imaging Research [NCMIR], University of California, San Diego, La

Jolla, CA). The mitochondrial reconstructions were visualized by Analyze (Mayo Foundation, Rochester, MN) or the surface-rendering graphics of Synu (NCMIR), as described by Perkins et al.[38] These programs allow one to step through slices of the reconstruction in any orientation and to track or model features of interest in three dimensions. Movies of the tomographic volume were constructed (Amira; Visage Imaging, Inc., Carlsbad, CA).

Quantitative PCR

Eight ONHs (extending 0.25 mm posteriorly from retina surface) were dissected from the sclera of four 3-month-old DBA/2J mice and four 10-month-old glaucomatous DBA/2J mice, as well as four 10-month-old nonglaucomatous C57BL/6 mice. The tissues were stored in preservative (RNA-later; Ambion, Inc., Austin, TX) at −20°C. Total RNA of pooled ONH from each group was extracted (TriZol; Invitrogen, Carlsbad, CA), purified on RNeasy mini columns (Qiagen, Valencia, CA), and treated with RNase-free DNase I (Qiagen). The RNA purity was verified by confirming that the optic density 260 nm/280 nm absorption ratio exceeded 1.9. cDNA was synthesized (SuperScript II first-strand RT-PCR kit; Invitrogen). COX, OPA1, and Dnm1 gene expression were measured by qPCR (MX3000P; Stratagene, La Jolla, CA) using 25 ng of cDNA from ONHs and 2× universal PCR master mix (*Taq*Man; Applied Biosystems, Inc., Foster City, CA) with a one-step program (95°C for 10 minutes, 95°C for 30 seconds, and 60°C for 1 minute for 50 cycles). Primers for COX, OPA1, Dnm1, and GAPDH, as well as a probe for GAPDH were designed on computer (Table 1; Primer Express 2.0 software; Applied Biosystems, Inc.). The probes for COX, OPA1, and Dnm1 were obtained from the Roche Universal Probe Library (Roche Diagnostics, Mannheim, Germany; Table 1), and the optimal concentrations for probe and primers were determined using heart tissue. Standard curves were constructed using nine twofold dilutions (50–0.195 ng) for both the targets (COX, OPA1, and Dnm1) and the endogenous reference (GAPDH). The samples were run in triplicate for each target and endogenous GAPDH control.

Western Blot Analysis

Six whole ONs (extending from ONH to optic chiasmatic nucleus) were dissected from the sclera of three 3-month-old DBA/2J mice, 8-month-old glaucomatous DBA/2J mice, and 10-month-old glaucomatous DBA/2J mice. Tissues are then immediately homogenized in a glass-Teflon Potter homogenizer in lysis buffer (20 mM HEPES [pH 7.5], 10 mM KCl, 1.5 mM $MgCl_2$, 1 mM EDTA, 1 mM EGTA, 1 mM DTT, 0.5% CHAPS, and complete protease inhibitors; Roche Biochemicals, Indianapolis, IN). Ten micrograms of pooled samples from each group were separated by PAGE and electrotransferred to PVDF membranes. The membrane was blocked with 5% nonfat dry milk, 0.05% Tween-20, PBS, incubated with monoclonal mouse anti-OPA1 antibody (H-300/1:1000; BD Transduction Laboratories, San Diego, CA) or monoclonal mouse anti-actin antibody (Ab-1/1:3000; Calbiochem, La Jolla, CA), rinsed with 0.05% Tween-20/PBS, incubated with peroxidase-conjugated goat anti-mouse IgG (1:2000; Bio-Rad, Hercules, CA) or goat anti-rabbit IgM (1:5000; Calbiochem), and developed with chemiluminescence detection (ECL Plus; GE Healthcare, Piscataway, NJ). Images were analyzed by digital fluorescence imager (Storm 860; GE Healthcare), and band densities were normalized by using actin as cytosolic fraction calibrator and VDAC as a mitochondrial fraction calibrator (ImageQuant TL; GE Healthcare).

To assess the subcellular distribution of OPA1, the cytosolic and mitochondrial fractions were extracted from freshly isolated ONs by differential centrifugation (Mitochondrial Isolation Kit; Pierce Biotechnology, Rockford, IL). Briefly, the tissues were immediately homogenized in a glass-Teflon Potter homogenizer in reagent A, mixed with an equal volume of reagent C, and then centrifuged at 700*g* for 10 minutes at 4°C. For the cytosolic fraction, the supernatant was centrifuged at 12,000*g* for 15 minutes at 4°C, and the supernatant was collected as the cytosolic fraction. For the mitochondrial fraction, the mitochondrial pellet was lysed with 2% CHAPS in Tris-buffered saline and centrifuged at 12,000*g* for 15 minutes at 4°C, and the supernatant was collected. Western blot analysis was performed as just described. Equal loading was confirmed by reprobing cytosolic fraction samples with actin, and the mitochondrial fraction samples with polyclonal rabbit anti-VDAC antibody (Ab-5/1:1000; Calbiochem). Band densities were normalized by using actin as cytosolic fraction calibrator and VDAC as mitochondrial fraction calibrator (ImageQuant TL; GE Healthcare). Good separation of the cytosolic and mitochondrial fractions was confirmed by the observation of negligible staining when cytosolic fraction blots were reprobed with antibodies to VDAC and when mitochondrial fraction blots were reprobed with antibodies to actin (data not shown).

Statistical Analysis

Experiments presented were repeated at least three times with triplicate samples. The data are presented as the mean ± SD. Comparison of two experimental conditions was evaluated using the unpaired Student's *t*-test. $P < 0.05$ was considered to be statistically significant.

Results

Elevated IOP–Induced Mitochondrial Fission and Cristae Depletion in the ONH

Mean IOP was 15 ± 1.8 mm Hg (SD) in 3-month-old DBA/2J mice. Spontaneous IOP elevation typically began by 6 to 8 months. The peak of IOP elevation was 21.5 ± 4.5 mm Hg in the right eyes and 19.9 ± 3.7 mm Hg in the left eyes within 10-month-old DBA/2J mice (Fig. 1). In contrast, mean IOP was

Table 1. Primer and Probe Sequences for Mouse COX, OPA1, Dnm1, and GAPDH for qPCR

Gene (Accession No.)	Type	Sequences (5′–3′)
COX (NM_009941)	Forward	TCACTGCGCTCGTTCTGAT
Roche Applied Science	Reverse	CGATCGAAAGTATGAGGGATG
	Probe	Universal Probe Library probe 7; Cat. 04685059001
OPA1 (NM_133752)	Forward	TGACAAACTTAAGGAGGCTGTG
Roche Applied Science	Reverse	CATTGTGCTGAATAACCCTCAA
	Probe	Universal Probe Library probe 91; Cat. 04692080001
Dnm1 (NM_010065)	Forward	CGGTTAGACAGTGCACCAAG
Roche Applied Science	Reverse	GGATGTGGGTGGTCACAAT
	Probe	Universal Probe Library probe 52; Cat. 04688490001
GAPDH (NM_008084)	Forward	CAACGGGAAGCCCATCAC
	Reverse	CGGCCTCACCCCATTTG
	Probe	CTTCCAGGAGCGAGACCCCACTAACA

*Taq*man (ABI, Foster City, CA) probe containing 5′ reporter FAM and 3′ quencher BHQ-1 dyes (in parentheses, GeneBank accession numbers; http://www.ncbi.nlm.nih.gov/Genbank; provided in the public domain by the National Center for Biotechnology Information, Bethesda, MD).

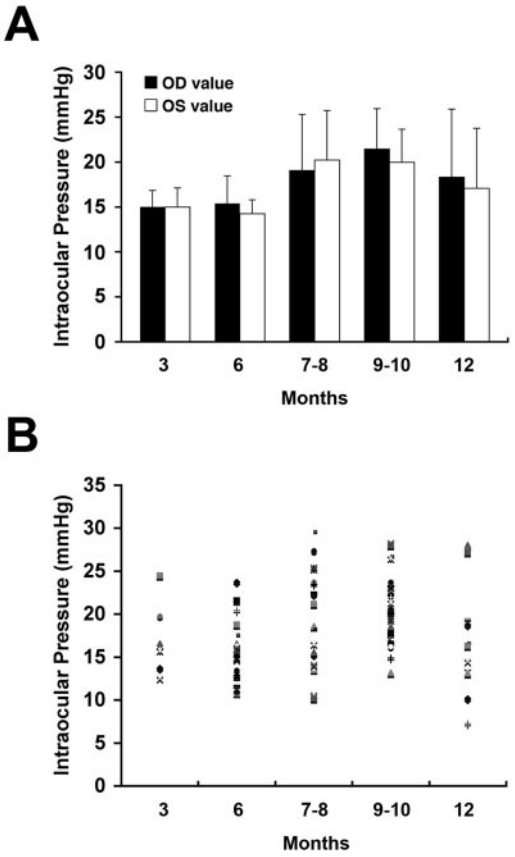

FIGURE 1. IOP elevation in glaucomatous DBA/2J mice. (**A**) The average IOP and (**B**) representative actual IOPs in eyes of mice aged 3, 6, 7–8, 9–10, and 12 months. The peak of IOP elevation was 21.5 ± 4.5 mm Hg in the right eyes and 19.9 ± 3.7 mm Hg in the left eyes in the 10-month-old mice.

14.7 ± 1.7 mm Hg in the right eyes and 14.2 ± 1.8 mm Hg in the left eyes in the 10-month-old nonglaucomatous C57BL/6 mice (see Supplementary Fig. S1; all supplementary figures are online at http://www.iovs.org/cgi/content/full/49/11/4903/DC1). To evaluate ON degeneration and axon loss, we analyzed cross and longitudinal sections stained with toluidine blue. The ONs in these mice had a normal appearance at 3 months of age (Figs. 2A, 2C, 2E). As has been reported previously,[28,42] substantial ON damage, including axon loss, was observed in 10-month-old glaucomatous DBA/2J mice (Figs. 2B, 2D, 2F), confirming the presence of acquired optic neuropathy.

Mitochondrial distribution and structure were compared in the ONH of 3-month-old DBA/2J mice with normal IOP and 10-month-old glaucomatous DBA/2J mice with confirmed IOP elevation (>20 mm Hg). As shown in Figure 3, COX immunoreactivity, a marker for mitochondria activity,[43–45] was concentrated in the unmyelinated ONH of 3-month-old DBA/2J mice (Fig. 3A). In contrast, much less COX immunoreactivity was observed in the unmyelinated ONH of 10-month-old glaucomatous DBA/2J mice (Fig. 3B; see three more examples in Supplementary Fig. S2). qPCR with specific primers (*Taq*Man; ABI) and probes for mouse COX showed that COX mRNA was significantly decreased by 0.81 ± 0.06-fold in the ONHs of 10-month-old DBA/2J glaucomatous mice compared with that in the ONHs of 3-month-old DBA/2J mice ($n = 8$ ONHs per pool, Fig. 3C, $P < 0.05$). In addition, COX mRNA was decreased by 0.9 ± 0.04-fold in the ONHs of 10-month-old C57BL/6 mice compared with that in the ONHs of 3-month-old mice ($n = 8$ ONHs per pool, Fig. 3C). There were insignificant differences in COX mRNA expression relative to GAPDH mRNA or in the ratios of GAPDH mRNA to total RNA between the 3-month-old DBA/2J mice ONHs and 10-month-old C57BL/6 mice ONHs (data not shown).

Transmission EM analysis showed that the axons of the unmyelinated ONH in 3-month-old DBA/2J mice contained classic elongated tubular mitochondria of various lengths (Fig. 3D). In contrast, 10-month-old glaucomatous DBA/2J mice unmyelinated ONH axons contained small rounded mitochondria with swollen matrices (Fig. 3E; see four more examples in Supplementary Fig. S3).

A power analysis was employed on the measured mitochondrial lengths from the 3- and 10-month-old samples with the expectation that mitochondrial fission would be statistically significant. The null hypothesis is that the mean lengths of the 3- and 10-month-old mitochondria are equal. We chose the type I error rate (a) to be low (0.001). This is the probability of incorrectly rejecting a true statistical null hypothesis, a "false positive." We desired the type II error rate (b), a "false negative," to be kept low as well, so that the "statistical power," equal to $1 - b$, be kept correspondingly high. For the given effect size (population means of 858 nm and 583 nm, and standard deviations of 515 nm and 299 nm for the 3- and 10-month-old samples, respectively), sample sizes ($n = 1016$ and 1023 for the 3- and 10-month-old samples, respectively), and a (0.001, 2 tailed), the power was calculated to be 1.0 (Fig. 3F). This power value means that close to 100% of studies would be expected to yield a significant difference in mean

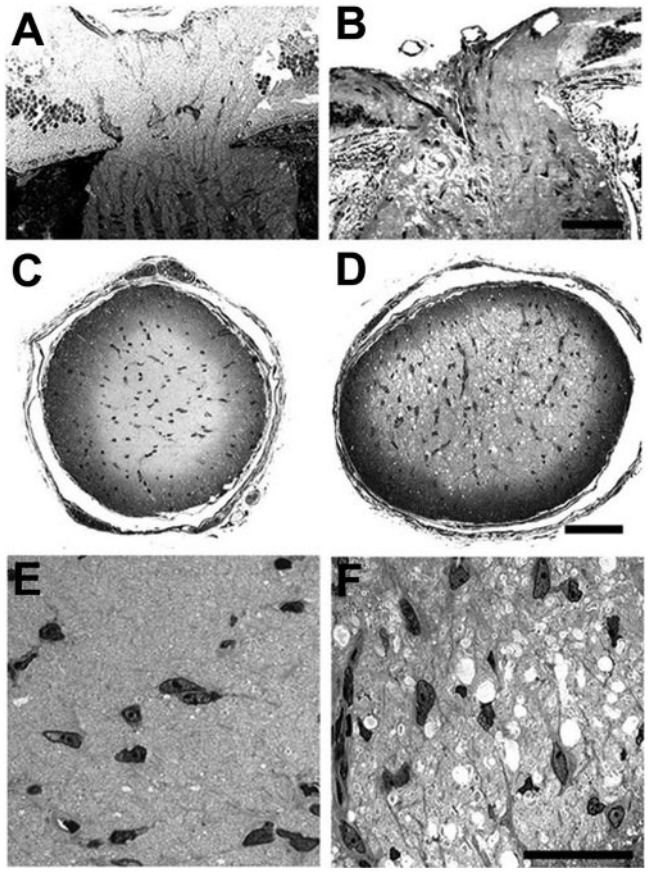

FIGURE 2. ON degeneration in glaucomatous DBA/2J mice. (**A**, **C**, **E**) The ON of 3-month-old mice. (**B**, **D**, **F**). The ON of 10-month-old glaucomatous mice. Note degenerated ONH (**B**) and ON axon loss (**D**, **F**) in the ON of 10-month-old glaucomatous mice with elevated IOP. The specimen preservation procedure was optimized for mitochondria preservation. Scale bars: (**A**–**D**) 50 μm; (**E**, **F**) 20 μm.

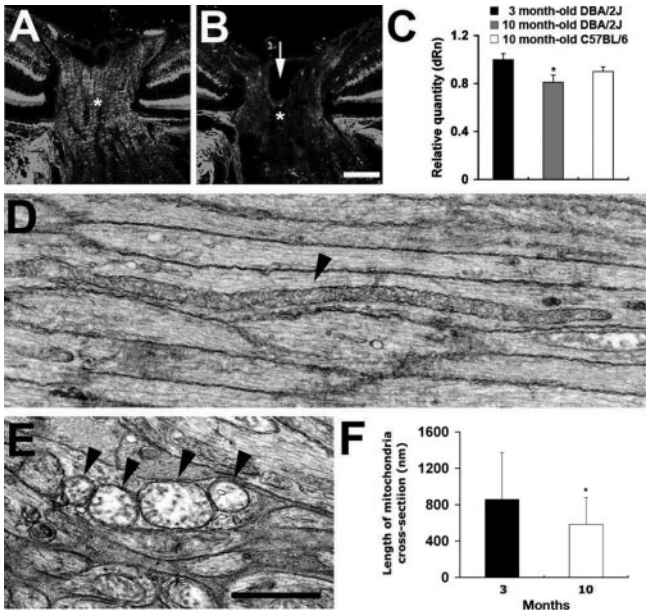

FIGURE 3. Mitochondrial fission, matrix swelling, and cristae depletion in the unmyelinated ONH of glaucomatous DBA/2J mice. (**A**, **B**) COX immunohistochemistry in the unmyelinated ONH. COX immunoreactivity was concentrated in the unmyelinated ONH of 3-month-old DBA/2J mice (**A**, ✶). In contrast, much less COX immunoreactivity was observed in the unmyelinated ONH of 10-month-old glaucomatous DBA/2J mice (**B**, ✶, *arrow*). The sections were counterstained with the nucleic acid stain Hoechst 33342 (*blue*). (**C**) COX mRNA expression was significantly decreased in the ONHs of 10-month-old glaucomatous DBA/2J mice ($^*P < 0.05$ by Student's *t*-test, $n = 3$ for both 3- and 10-month-old mice) but there are no significant changes between 3-month-old DBA/2J mice and 10-month-old nonglaucomatous C57BL/6 mice. (**D**, **E**) Ultrastructural changes of mitochondria in the unmyelinated ONH. Three-month-old mice had elongated mitochondria of various lengths showing normal matrix and membrane structures (**D**, *arrowhead*). In contrast, mitochondria from 10-month-old glaucomatous mice with IOP elevation (**E**, *arrowheads*) had small rounded organelles and significant matrix swelling. (**F**) Quantitative analysis of mitochondrial lengths in the unmyelinated ONH. Using conventional thin-section EM, the length of mitochondrial cross sections at the longest extent was measured from 2-D projection images. Error bar, SD ($^*P < 0.001$, $n = 1016$ and 1023 for 3- and 10-month-old mice, respectively). Scale bar: (**A**, **B**) 50 μm; (**D**, **E**) 1 μm.

mitochondrial lengths from the 3- and 10-month-old populations, rejecting the null hypothesis that the means are equal.

To assess the internal mitochondrial structural changes, unmyelinated ONHs from 3- and 10-month-old DBA/2J mice were fixed to preserve mitochondrial morphology, and EM tomography was used to obtain 3-D reconstructions showing detailed mitochondrial ultrastructure. Tomographic reconstructions from a 3-month-old sample showed an intact outer mitochondrial membrane (blue) and mostly lamellar cristae (various colors), occupying the mitochondrial matrix space (Fig. 4A). By comparison, 3-D tomographic volumes of mitochondria found in axons of 10-month-old glaucomatous DBA/2J mice often showed smaller, more globular mitochondria that were occasionally in close proximity (Fig. 4B). Mitochondria of 10-month-old glaucomatous DBA/2J mice showed matrix swelling and substantially reduced cristae volume. Figures 4Ba and Bb show an example of a mitochondrion that was devoid of cristae in much of its volume and also displayed matrix swelling (lighter regions). Mitochondrial fission also was suggested in the tomographic reconstructions (Fig. 4B, arrowheads) because of the observation of closely apposed mitochondrial fragments.

Effect of IOP Elevation on OPA1 Gene and Protein Expression or Dnm1 Gene Expression in the ONH

OPA1 mutation or deficiency in mouse models causes RGC and nerve fiber layer degeneration, mitochondrial dysfunction, ON abnormalities, and visual deficits.[46,47] To test whether alteration of OPA1 protein expression occurs in the ONH of glaucomatous mice, OPA1 immunohistochemistry was performed. As shown in Figure 5, substantial OPA1 immunoreactivity was present in the ONH of 3-month-old DBA/2J mice (Fig. 5A).

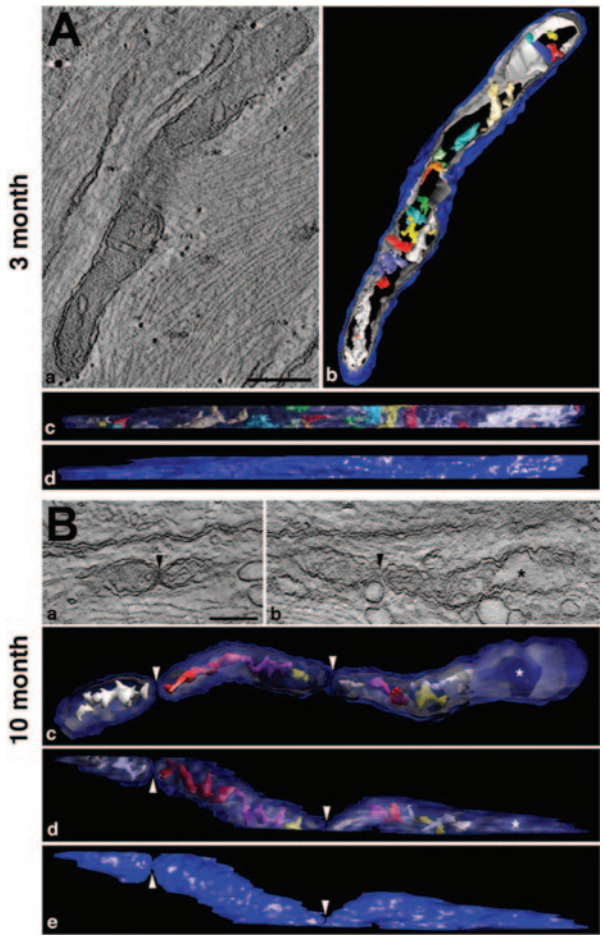

FIGURE 4. Three-dimensional reconstructions of mitochondria using EM tomography. Slices of 1.4-nm thickness through each reconstruction are shown through the middle of the 3-month ONH (**Aa**) and at two different heights through the 10-month-old ONH (**Aa**, **Bb**), to emphasize the normal structural features of the former and the fission and localized swelling of the latter. In the 10-month-old specimen, mitochondrial fission occurred in two places, giving three mitochondrial bodies. The two slices through the tomographic volume showing the closest apposition of left and middle bodies (**Ba**) and middle and right bodies (**Bb**) emphasize that fission was completed (*arrowheads*). Matrix swelling and lack of cristae were observed in a localized region of the right mitochondrial body (✶). Top (**Ab** and **Ac**) and side (**Ac**, **Ad**, **Bd**, **Be**) views of surface-rendered volumes of the mitochondria after segmentation of the membranes show the distribution of cristae and any subvolumes devoid of cristae. The outer membrane is shown in *blue* and made transparent in (**Ac**), (**Bc**), and (**Bd**), to make the shapes and sizes of the cristae easily visible. The cristae are shown in various colors. Side views of the outer membrane show no ruptures of this membrane (**Ad**, **Be**). *Arrowheads*: fission loci that are seen in (**Be**). The subvolume with swollen matrix and devoid of cristae is also marked in (**Ac**) and (**Bd**) (✶). Scale bar, 200 nm. See Movies S1 and S2, online at http://www.iovs.org/cgi/content/full/49/11/4903/DC1.

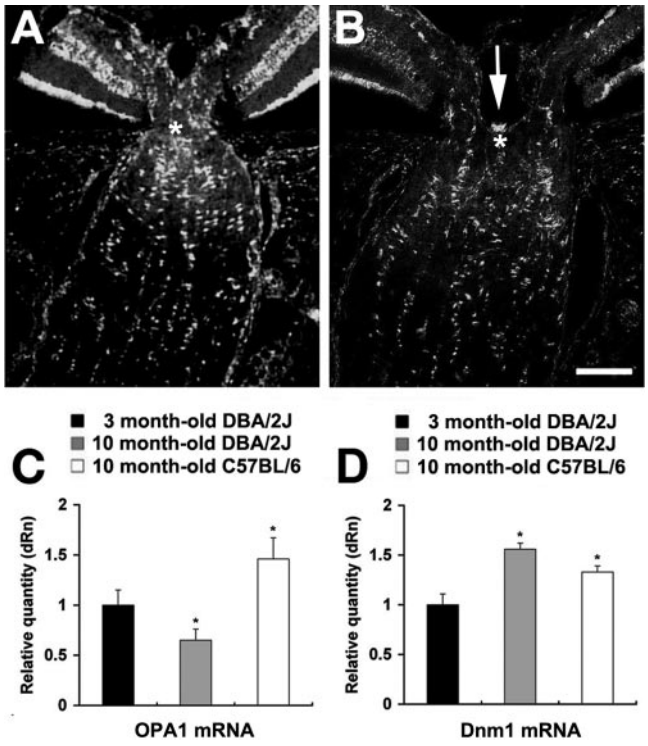

FIGURE 5. Alterations of OPA1 protein and gene expression or Dnm1 gene expression in the ONH of glaucomatous DBA/2J mice. (**A**, **B**) OPA1 immunohistochemistry in the unmyelinated ONH. OPA1 immunoreactivity was concentrated in the ONH of 3-month-old mice (**A**, ✶). In contrast, much less OPA1 immunoreactivity was observed in the ONH of 10-month-old glaucomatous mice (**B**, ✶, *arrow*). The sections were counterstained with the nucleic acid stain Hoechst 33342 (*blue*). (**C**) Reduction of OPA1 mRNA expression in the ONHs of 10-month-old glaucomatous DBA/2J mice. Ten-month-old glaucomatous DBA/2J mice showed a significant reduction of OPA1 mRNA expression in the ONHs. In contrast, 10-month-old nonglaucomatous C57BL/6 mice showed a significant increase of OPA1 mRNA expression in the ONHs. (**D**) Increase of Dnm1 mRNA expression in the ONHs of 10-month-old glaucomatous DBA/2J mice. Both 10-month-old glaucomatous DBA/2J and 10-month-old nonglaucomatous C57BL/6 mice showed a significant increase in Dnm1 mRNA expression in the ONHs. Error bar, SD (*$P < 0.05$ by Student's *t*-test, $n = 3$ for both 3- and 10-month-old mice). Scale bar: (**A**, **B**) 50 μm.

Much less OPA1 immunoreactivity was observed in the ONH of 10-month-old glaucomatous DBA/2J mice than in the 3-month-old DBA/2J mice (Fig. 5B; see four more examples in Supplementary Fig. S4). To determine whether there were differences in the expression of mRNA for OPA1 and Dnm1 (a mouse homologue of Drp-1) associated with advancing glaucomatous damages, qPCR was performed on ONH mRNA from 3-month-old DBA/2J mice and 10-month-old glaucomatous DBA/2J mice, as well as 10-month-old nonglaucomatous C57BL/6 mice. The results were normalized to GAPDH mRNA. We observed that OPA1 mRNA was decreased by 0.65 ± 0.11-fold in the ONHs of 10-month-old glaucomatous DBA/2J mice but was increased by 1.46 ± 0.21-fold in the ONHs of 10-month-old nonglaucomatous C57BL/6 mice ($n = 8$ ONHs per pool; Fig. 5C; both significant increases at $P < 0.05$). This result is consistent with increased mitochondrial fission in the 10-month-old glaucomatous DBA/2J mice described earlier. In contrast, Dnm1 mRNA was increased by 1.56 ± 0.06-fold in the ONHs of 10-month-old glaucomatous DBA/2J mice and by 1.33 ± 0.06-fold in the ONHs of 10-month-old nonglaucomatous C57BL/6 mice ($n = 8$ ONHs per pool, Fig. 5D, both significant increases at $P < 0.05$). There were no differences in the ratios of GAPDH mRNA to total RNA among the 3-month-old DBA/2J mice ONHs, 10-month-old glaucomatous DBA/2J mice ONHs and 10-month-old C57BL/6 mice ONHs (data not shown).

Elevated IOP–Induced Mitochondrial OPA1 Release in the ON

To investigate possible OPA1 translocation from mitochondria to the cytosol in the whole ONs of 8- and 10-month-old glaucomatous mice, relative changes of OPA1 concentration in cytosolic and mitochondrial fractions were measured by Western blot analysis. The blots were reprobed with actin and

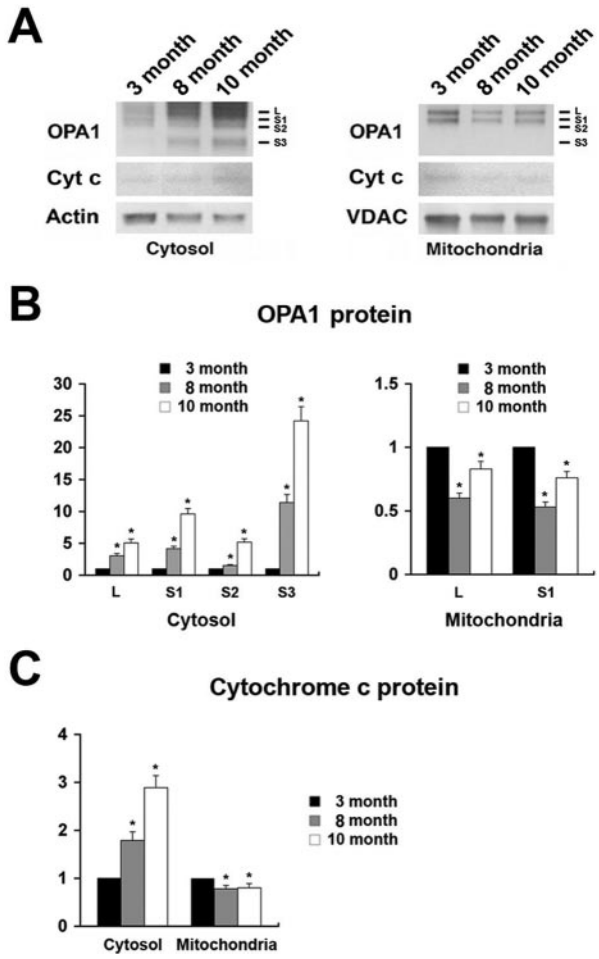

FIGURE 6. Alteration of OPA1 distribution in the ONs of glaucomatous DBA/2J mice. (**A**) OPA1 Western blot analysis of cytosolic and mitochondrial fractions from whole ONs. The OPA1 protein bands show the positions of three major isoforms of OPA1 (90 kDa, L; 80 kDa, S1; 75 kDa, S2). There was a fourth isoform of OPA1 protein band (~65 kDa, S3) in the cytosolic fraction of the ONs in the 8- and 10-month-old glaucomatous mice. The cytochrome *c* protein bands show the positions of the 17-kDa form of cytochrome *c* in the cytosolic and mitochondrial fraction. (**B**) Relative intensity of chemiluminescence for each protein band was normalized using actin (~42 kDa) as the cytosolic fraction calibrator and VDAC (~31 kDa) as the mitochondrial fraction calibrator. The L, S1, and S2 isoforms of OPA1 were significantly increased in the cytosolic fraction. In contrast, the L and S1 isoforms of OPA1 were significantly decreased in the mitochondrial fraction in the 8- and 10-month-old glaucomatous mice. The cytochrome *c* protein bands were significantly increased in the cytosolic fraction. However, the cytochrome *c* protein band was decreased in the mitochondrial fraction in the 8- and 10-month-old glaucomatous mice. Error bar, SD (*$P < 0.05$ by Student's *t*-test, $n = 3$ for 3-, 8-, and 10-month-old mice).

VDAC antibody, to assess protein loading in the lanes containing cytosolic or mitochondrial proteins, respectively. Results were normalized to actin as a cytosolic fraction calibrator and VDAC as a mitochondrial fraction calibrator. As shown in Figure 6A, the OPA1 antibody recognized three major OPA1 isoforms: a 90-kDa (called the large or L form), an 80-kDa (S1), and a 75-kDa (S2) isoform in the cytosolic fraction of 3-month-old DBA/2J mouse ONs. Two major isoforms (L and S1) were identified in the mitochondrial fraction of 3-month-old mouse ON. In contrast, 8- and 10-month-old glaucomatous mouse ONs contained at least four isoforms of OPA1 in the cytosolic fractions, including a small isoform (~65 kDa:S3). Moreover, relative OPA1 content of all four isoforms was significantly increased by 3.05 ± 0.35-fold (L), 4.15 ± 0.39-fold (S1), 1.52 ± 0.16-fold (S2), and 11.4 ± 1.25-fold (S3) in the ONs of 8-month-old and by 5.06 ± 0.62-fold (L), 9.61 ± 0.85-fold (S1), 5.19 ± 0.53-fold (S2), and 24.2 ± 2.23-fold (S3) in the ONs of 10-month-old glaucomatous mice ($P < 0.05$, Figs. 6A, 6B). Concomitantly, relative OPA1 content of both mitochondrial isoforms (L and S1) were decreased by 0.60 ± 0.04-fold (L) and 0.53 ± 0.04-fold (S1) in the ONs of 8-month-old and by 0.79 ± 0.06-fold (L) and 0.76 ± 0.05-fold (S1) in the ONs of 10-month-old glaucomatous mice, respectively (both significant decreases at $P < 0.05$, Figs. 6A, 6B).

Cytochrome *c* protein concentration was significantly increased (1.79 ± 0.18- and 2.89 ± 0.3-fold) in the cytosolic fraction of the ONs of 8- and 10-month-old glaucomatous mice, respectively ($P < 0.05$, Figs. 6A, 6C). In contrast, the cytochrome *c* protein concentration was significantly decreased (by 0.78 ± 0.06- and 0.80 ± 0.07-fold in the mitochondrial fraction of the ONs of 8- and 10-month-old glaucomatous mice, respectively ($P < 0.05$, Figs. 6A, 6C).

Discussion

These results demonstrate that the ON degeneration that occurs in glaucomatous DBA/2J mice with elevated IOP induces COX reduction, mitochondrial fission, and abnormal cristae depletion, alterations of OPA1 and Dnm1 expression, and induction of OPA1 release. These findings suggest that mitochondrial dysfunction contributes to the biochemical cascade leading to pressure-related RGC axon loss and ON degeneration in glaucoma.

Growing evidence indicates that mitochondrial structural and functional dynamics play an important role in cell and animal physiology. Imbalance in the control of mitochondrial fusion and fission dramatically alters overall mitochondrial morphology.[9] In addition, recent evidence suggests that excessive mitochondrial fission can lead to breakdown of the mitochondrial network, loss of mitochondrial DNA, and respiratory defects in mammalian cells.[48–50] Previously, we reported that elevated hydrostatic pressure caused breakdown of the mitochondrial network by mitochondrial fission and induced abnormal cristae depletion and cellular ATP reduction in differentiated RGC-5 cells in vitro.[5] This suggests that these cells may have bioenergetic impairment.[5,37,39,51] The present results extend these findings in an in vivo model. The mean length of mitochondrial cross section significantly decreased in the unmyelinated ONH of 10-month-old glaucomatous mice, suggesting mitochondrial fission. In addition, EM tomography showed matrix swelling and substantially reduced cristae volume, including regions devoid of cristae, providing even stronger evidence of mitochondrial fission by allowing much more of the volume to be visualized than afforded by conventional EM. The depletion of cristae membranes is consistent with our finding of reduced COX expression in the ONH of 10-month-old glaucomatous mice. Further, the finding that Dnm1 expression increased is reflected in the increased mitochondrial fission observed. These alterations to the 3-D structure observed in 10-month-old glaucomatous mice mitochondria argue for reduced ATP generation and general mitochondrial dysfunction. Recent studies suggest that mitochondrial distribution in the ONH reflects differing energy requirements of the unmyelinated axons in comparison to the myelinated retrolaminar axons (i.e., the unmyelinated portion of the ON may have greater demands for mitochondrially derived ATP than does the myelinated posterior nerve).[52–54] Also, deficiency in mitochondrially derived ATP triggers RGC death in Leber's hereditary optic neuropathy.[55] Together with these findings, our observations suggest that the mitochondrial dysfunction in the ONH is important during the onset of glaucomatous optic neuropathy.

In the present study, IOP elevation significantly decreased OPA1 mRNA and protein expression in the ONH of 10-month-old glaucomatous mice. Recent studies have demonstrated that OPA1 protein is present in the ONH of the rat and human as well as in the RGCs of the mouse, rat, and human retinas[12–15]; that downregulation of OPA1 causes aggregation of the mitochondrial network in purified RGCs[19]; and that these changes are linked to mitochondrial fission, mitochondrial cristae depletion, and bioenergetic impairment.[16,17,22] Because OPA1 deficiency in mouse models of ADOA impairs mitochondrial morphology, ON structure, and visual function,[46,47] the observed reduction of OPA1 gene and protein expression in the ONH of 10-month-old glaucomatous mice with IOP elevation appears to be reflected in the structural and functional changes of mitochondria and may facilitate ONH axon loss. Further support for this idea comes from studies showing that increased OPA1 expression protects cells from apoptosis by preventing cytochrome *c* release and by stabilizing the shape of mitochondrial cristae.[21,56]

In contrast to OPA1, IOP elevation significantly increased Dnm1 mRNA expression in the ONHs of 10-month-old glaucomatous mice. Recent evidence indicates that mitochondrial fission is associated with the translocation of Drp-1 from cytoplasm to defined spots on the mitochondrial membrane.[9,49,57–59] Consistent with these prior studies, we reported that Drp-1 protein was decreased in the cytosolic fraction in the pressure-treated cells but was increased in the mitochondrial fraction, indicating that Drp-1 translocation into mitochondria in our model contributes to the mechanism of mitochondrial fission in differentiated RGC-5 cells in vitro after elevated hydrostatic pressure.[5] Further evidence has suggested that inhibiting Drp-1-mediated mitochondrial fission selectively prevents the release of cytochrome *c* during apoptosis.[60] Together with these findings, the current results suggest that increase of ONH Dnm1 expression by IOP elevation may also lead to structural and functional changes of mitochondria that facilitate ON axon loss. Thus, treatments that enhance OPA1 retention in mitochondria or that inhibit Drp-1 mediated mitochondrial fission may provide a new strategy to protect against ON degeneration and RGC loss in glaucoma.

Nonglaucomatous 10-month-old C57BL/6 mice were included in our evaluations of COX, OPA1, and Dnm1 mRNA expression as an age-matched normal control strain. The absence of IOP elevation with age was confirmed (shown in Supplementary Fig. S1). Although several mitochondrial changes occur with old age, senescence, or apoptosis, there appear to be minimal differences in neuronal mitochondria from 4-month-old young-mature rats and 13-month-old middle-aged rats.[61] Thus, it is unlikely that there are significant differences in neuronal mitochondria of young mature normal mice (3-month-old) and middle-aged normal mice (10-month-old). Comparison of the results from the 10-month-old C57BL/6 mice with the 3- and 10-month-old DBA/2J mice results found COX mRNA was greatest in the 3-month-old DBA/2J mouse ONHs, 0.90-fold less in the 10-month-old C57BL/6 mouse

ONHs, and 0.81-fold less in the 10-month-old DBA/2J mouse ONHs. This result may merely reflect fewer axons in the ONHs of the latter two groups, as it is consistent with previous reports of modest age-related axon loss in normal C57BL/6 mice[62] as well as accelerated axon loss in mice with elevated IOP.[27,42,63–65] Relative to OPA1 mRNA in the ONHs of 3-month-old DBA/2J mice, OPA1 mRNA was 0.65-fold less in glaucomatous 10-month-old DBA/2J mice but 1.46-fold greater in the nonglaucomatous 10-month-old C57BL/6 mice. Because these differences were greater in magnitude than the corresponding differences in COX mRNA, they suggest a positive association between IOP elevation and reduced expression of the OPA1 gene. Moreover, they raise the possibility that OPA1 mRNA expression changes precede IOP-associated axon loss. In contrast to OPA1, expression of Dnm1 mRNA (which codes for a protein that promotes mitochondrial fission), was least in the 3-month-old DBA/2J mouse ONHs and greatest in the 10-month-old DBA/2J mouse ONHs. This finding is consistent with an important role for IOP. The intermediate expression of Dnm1 mRNA in the 10-month-old C57BL/6 mouse ONHs may reflect the more robust expression of OPA1 mRNA in this strain than in the 3-month-old DBA/2J mice. Together, these results support important influences of both normal aging and elevated IOP on the transition of mitochondrial fission/fusion balance to favor fission.

OPA1 release during mitochondrial fission participates in apoptotic cell death.[18,22] Consistent with these prior studies, we found that elevated hydrostatic pressure triggers release of OPA1 and cytochrome *c* and induces subsequent apoptotic cell death in differentiated RGC-5 cells in vitro (Ju WK, et al. *IOVS* 2007;48:ARVO E-Abstract 5551). In the present study, IOP elevation gradually induced OPA1 release from mitochondria to the cytosol in the ONs of 8- and 10-month-old glaucomatous mice. The actin-normalized concentrations of each of the four OPA1 isoforms present in the cytosol from 8-month-old ONs were intermediate between the results at 3 months of age and the results at 10 month of age. This finding shows the progressive nature of the increase in cytosolic OPA1 that manifest during the progression of glaucomatous damage and is further supported by the progressive increase in cytosolic cytochrome *c* seen in 3-, 8-, and 10-month-old DBA/2J mice. The greater reduction in the VDAC-normalized concentration of the two OPA1 isoforms in the mitochondrial fraction may reflect that mitochondrial OPA1 changes are more dramatic and precede the changes in cytosolic OPA1 and axon survival. In contrast, mitochondrial cytochrome *c* is reduced similarly at 8 and 10 months of age. Hence, it is possible that OPA1 release in glaucomatous ON with IOP elevation contributes directly to ON axon loss by mediating abnormal mitochondrial structural impairment. In addition to evidence of OPA1 release to the cytoplasm, a small immunoreactive band (~65 kDa) appeared in the cytosolic fraction in the ONs of the eyes with IOP elevation. A rhomboid intramembrane protease PARL cleaves the OPA1 protein, and the cleavage of OPA1 generates a pool of truncated OPA1 that is soluble in the intermembrane space.[66] Moreover, the soluble OPA1 may be crucial for the anti-apoptotic effects of PARL, because it maintains the bottleneck configuration of cristae and the compartmentalization of cytochrome *c*.[21,66] Thus, it is likely that the unexpected low molecular weight of OPA1 fragments presently observed include the truncated forms of OPA1 that localize to the intermembrane space or possibly one of the degradation products. The functional contributions of each of the various soluble OPA1 isoforms that are released from ON mitochondria after IOP elevation should be explored further.

In summary, IOP elevation induces reduction of COX activity, mitochondrial fission, mitochondrial matrix swelling, and cristae depletion, alterations of OPA1 and Dnm1 expression, and induction of OPA1 release from mitochondria in glaucomatous ON. Thus, these findings support the idea that interventions to protect against mitochondrial fission-related dysfunction may be beneficial for reducing glaucomatous ON degeneration and RGC loss.

Acknowledgments

The authors thank Simon W. M. John (The Jackson Laboratory, Bar Harbor, ME) for helpful comments on the manuscript.

References

1. Weinreb RN, Khaw PT. Primary open-angle glaucoma. *Lancet*. 2004;363(9422):1711–1720.
2. Brenner C, Kroemer G. Apoptosis. Mitochondria-the death signal integrators. *Science*. 2000;289(9482):1150–1151.
3. Kroemer G, Reed JC. Mitochondrial control of cell death. *Nat Med*. 2000;6(5):513–519.
4. Abu-Amero KK, Morales J, Bosley TM. Mitochondrial abnormalities in patients with primary open-angle glaucoma. *Invest Ophthalmol Vis Sci*. 2006;47(6):2533–2542.
5. Ju WK, Liu Q, Kim KY, et al. Elevated hydrostatic pressure triggers mitochondrial fission and decreases cellular ATP in differentiated RGC-5 cells. *Invest Ophthalmol Vis Sci*. 2007;48(5):2145–2151.
6. Nunnari J, Marshall WF, Straight A, Murray A, Sedat JW, Walter P. Mitochondrial transmission during mating in Saccharomyces cerevisiae is determined by mitochondrial fusion and fission and the intramitochondrial segregation of mitochondrial DNA. *Mol Biol Cell*. 1997;8(7):1233–1242.
7. Karbowski M, Youle RJ. Dynamics of mitochondrial morphology in healthy cells and during apoptosis. *Cell Death Differ*. 2003;10(8):870–880.
8. Okamoto K, Shaw JM. Mitochondrial morphology and dynamics in yeast and multicellular eukaryotes. *Annu Rev Genet*. 2005;39:503–536.
9. Chen H, Chan DC. Emerging functions of mammalian mitochondrial fusion and fission. *Hum Mol Genet*. 2005;14:R283–R289.
10. Alexander C, Votruba M, Pesch UE, et al. OPA1, encoding a dynamin-related GTPase, is mutated in autosomal dominant optic atrophy linked to chromosome 3q28. *Nat Genet*. 2000;26(2):211–215.
11. Delettre C, Lenaers G, Griffoin JM, et al. Nuclear gene OPA1, encoding a mitochondrial dynamin-related protein, is mutated in dominant optic atrophy. *Nat Genet*. 2000;26(2):207–210.
12. Aijaz S, Erskine L, Jeffery G, Bhattacharya SS, Votruba M. Developmental expression profile of the optic atrophy gene product: OPA1 is not localized exclusively in the mammalian retinal ganglion cell layer. *Invest Ophthalmol Vis Sci*. 2004;45(6):1667–1673.
13. Pesch UE, Fries JE, Bette S, et al. OPA1, the disease gene for autosomal dominant optic atrophy, is specifically expressed in ganglion cells and intrinsic neurons of the retina. *Invest Ophthalmol Vis Sci*. 2004;45(11):4217–4225.
14. Ju WK, Misaka T, Kushnareva Y, et al. OPA1 expression in the normal rat retina and optic nerve. *J Comp Neurol*. 2005;488(1):1–10.
15. Wang AG, Fann MJ, Yu HY, Yen MY. OPA1 expression in the human retina and optic nerve. *Exp Eye Res*. 2006;83(5):1171–1178.
16. Olichon A, Baricault L, Gas N, et al. Loss of OPA1 perturbates the mitochondrial inner membrane structure and integrity, leading to cytochrome c release and apoptosis. *J Biol Chem*. 2003;278(10):7743–7746.
17. Lee YJ, Jeong SY, Karbowski M, Smith CL, Youle RJ. Roles of the mammalian mitochondrial fission and fusion mediators Fis1, Drp1, and Opa1 in apoptosis. *Mol Biol Cell*. 2004;15(11):5001–5011.
18. Arnoult D, Grodet A, Lee YJ, Estaquier J, Blackstone C. Release of OPA1 during apoptosis participates in the rapid and complete release of cytochrome c and subsequent mitochondrial fragmentation. *J Biol Chem*. 2005;280(42):35742–35750.
19. Kamei S, Chen-Kuo-Chang M, Cazevieille C, et al. Expression of the Opa1 mitochondrial protein in retinal ganglion cells: its downregu-

lation causes aggregation of the mitochondrial network. *Invest Ophthalmol Vis Sci*. 2005;46(11):4288–4294.
20. van der Bliek AM, Koehler CM. A mitochondrial rhomboid protease. *Dev Cell*. 2003;4(6):769–770.
21. Cipolat S, Rudka T, Hartmann D, et al. Mitochondrial rhomboid PARL regulates cytochrome c release during apoptosis via OPA1-dependent cristae remodeling. *Cell*. 2006;126(1):163–175.
22. Frezza C, Cipolat S, Martins de Brito O, et al. OPA1 controls apoptotic cristae remodeling independently from mitochondrial fusion. *Cell*. 2006;126(1):177–189.
23. Griparic L, Kanazawa T, van der Bliek AM. Regulation of the mitochondrial dynamin-like protein Opa1 by proteolytic cleavage. *J Cell Biol*. 2007;178(5):757–764.
24. John SW, Hagaman JR, MacTaggart TE, Peng L, Smithes O. Intraocular pressure in inbred mouse strains. *Invest Ophthalmol Vis Sci*. 1997;38(1):249–253.
25. John SW, Smith RS, Savinova OV, et al. Essential iris atrophy, pigment dispersion, and glaucoma in DBA/2J mice. *Invest Ophthalmol Vis Sci*. 1998;39(6):951–962.
26. Bhattacharya SK, Peachey NS, Crabb JW. Colchlin and glaucoma: a mini-review. *Vis Neurosci*. 2005;22(5):605–613.
27. Libby RT, Anderson MG, Pang IH, et al. Inherited glaucoma in DBA/2J mice: pertinent disease features for studying the neurodegeneration. *Vis Neurosci*. 2005;22(5):637–648.
28. Anderson MG, Libby RT, Mao M, et al. Genetic context determines susceptibility to intraocular pressure elevation in a mouse pigmentary glaucoma. *BMC Biol*. 2006;4:20.
29. Steele MR, Inman DM, Calkins DJ, Horner PJ, Vetter ML. Microarray analysis of retinal gene expression in the DBA/2J model of glaucoma. *Invest Ophthalmol Vis Sci*. 2006;47(3):977–985.
30. Huang W, Fileta JB, Filippopoulos T, Ray A, Dobberfuhl A, Grosskreutz CL. Hsp27 phosphorylation in experimental glaucoma. *Invest Ophthalmol Vis Sci*. 2007;48(9):4129–4135.
31. Nagaraju M, Saleh M, Porciatti V. IOP-dependent retinal ganglion cell dysfunction in glaucomatous DBA/2J mice. *Invest Ophthalmol Vis Sci*. 2007;48(10):4573–4579.
32. Howell GR, Libby RT, Jakobs TC, et al. Axons of retinal ganglion cells are insulted in the optic nerve early in DBA/2J glaucoma. *J Cell Biol*. 2007;179(7):1523–1537.
33. Aihara M, Lindsey JD, Weinreb RN. Reduction of intraocular pressure in mouse eyes treated with latanoprost. *Invest Ophthalmol Vis Sci*. 2002;43(1):146–150.
34. Misaka T, Miyahita T, Kubo Y. Primary structure of a dynamin-related mouse mitochondrial GTPase and its distribution in brain, subcellular localization, and effect on mitochondrial morphology. *J Biol Chem*. 2002;277(18):15834–15842.
35. von Ahsen O, Renken C, Perkins G, Kluck R, Bossy-Wetzel E, Newmeyer D. Preservation of mitochondrial structure and function after Bid- or Bax-mediated cytochrome c release. *J Cell Biol*. 2000;150(5):1027–1036.
36. Perkins GA, Renken CW, Frey TG, Ellisman MH. Membrane architecture of mitochondria in neurons of the central nervous system. *J Neurosci Res*. 2001;66(5):857–865.
37. Perkins GA, Ellisman MH, Fox DA. Three-dimensional analysis of mouse rod and cone mitochondrial cristae architecture: bioenergetic and functional implications. *Mol Vis*. 2003;9:60–73.
38. Perkins GA, Renken CW, Song JY, et al. Electron tomography of large, multicomponent biological structures. *J Struct Biol*. 1997;120(3):219–227.
39. Barsoum MJ, Yuan H, Gerencser AA, et al. Nitric oxide induced mitochondrial fission is regulated by dynamin related GTPase in neurons. *EMBO J*. 2006;25(16):3900–3911.
40. Kremer JR, Mastronarde DN, McIntosh JR. Computer visualization of three-dimensional image data using IMOD. *J Struct Biol*. 1996;116(1):71–76.
41. Lawrence A, Bouwer JC, Perkins GA, Ellisman MH. Transform-based backprojection for volume reconstruction of large format electron microscope tilt series. *J Struct Biol*. 2006;154(2):144–167.
42. Inman DM, Sappington RM, Horner PJ, Calkins DJ. Quantitative correlation of optic nerve pathology with ocular pressure and corneal thickness in the DBA/2 mouse model of glaucoma. *Invest Ophthalmol Vis Sci*. 2006;47(3):986–996.
43. Hevner RF, Wong-Riley MT. Regulation of cytochrome oxidase protein levels by functional activity in the macaque monkey visual system. *J Neurosci*. 1990;10(4):1331–1340.
44. Andrews RM, Griffiths PG, Johnson MA, Turnbull DM. Histochemical localisation of mitochondrial enzyme activity in human optic nerve and retina. *Br J Ophthalmol*. 1999;83(2):231–235.
45. Barron MJ, Griffiths P, Turnbull DM, Bates D, Nichols P. The distributions of mitochondria and sodium channels reflect the specific energy requirements and conduction properties of the human optic nerve head. *Br J Ophthalmol*. 2004;88(2):286–290.
46. Alavi MV, Bette S, Schimpf S, et al. A splice site mutation in the murine Opa1 gene features pathology of autosomal dominant optic atrophy. *Brain*. 2007;130:1029–1042.
47. Davies VJ, Hollins AJ, Piechota MJ, et al. Opa1 deficiency in a mouse model of autosomal dominant optic atrophy impairs mitochondrial morphology, optic nerve structure and visual function. *Hum Mol Genet*. 2007;16(11):1307–1318.
48. Yaffe MP. The machinery of mitochondrial inheritance and behavior. *Science*. 1999;283(5407):1493–1497.
49. Bossy-Wetzel E, Barsoum MJ, Godzik A, Schwarzenbacher R, Lipton SA. Mitochondrial fission in apoptosis, neurodegeneration and aging. *Curr Opin Cell Biol*. 2003;15(6):706–716.
50. Youle RJ, Karbowski M. Mitochondrial fission in apoptosis. *Nat Rev Mol Cell Biol*. 2005;6(8):657–663.
51. Mannella CA. Structure and dynamics of the mitochondrial inner membrane cristae. *Biochim Biophys Acta*. 2006;1763(5–6):542–548.
52. Rizzo JF III. Adenosine triphosphate deficiency: a genre of optic neuropathy. *Neurology*. 1995;45(1):1–16.
53. Bristow EA, Griffiths PG, Andrews RM, Johnson MA, Turnbul DM. The distribution of mitochondrial activity in relation to optic nerve structure. *Arch Ophthalmol*. 2002;120:791–796.
54. Carelli V, Ross-Cisneros FN, Sadun AA. Mitochondrial dysfunction as a cause of optic neuropathies. *Prog Retin Eye Res*. 2004;23(1):53–89.
55. Brown MD, Voljavec AS, Lott MT, MacDonald I, Wallace DC. Leber's hereditary optic neuropathy: a model for mitochondrial neurodegenerative diseases. *FASEB J*. 1992;6(10):2791–2799.
56. Ishihara N, Fujita Y, Oka T, Mihara K. Regulation of mitochondrial morphology through proteolytic cleavage of OPA1. *EMBO J*. 2006;25(13):2966–2977.
57. Karbowski M, Lee YJ, Gaume B, et al. Spatial and temporal association of Bax with mitochondrial fission sites, Drp1, and Mfn2 during apoptosis. *J Cell Biol*. 2002;159(6):931–938.
58. Frank S, Gaume B, Bergmann-Leitner ES, et al. The role of dynamin-related protein 1, a mediator of mitochondrial fission, in apoptosis. *Dev Cell*. 2001;1(4):515–525.
59. Chan DC. Mitochondrial fusion and fission in mammals. *Annu Rev Cell Dev Biol*. 2006;22:79–99.
60. Estaquier J, Arnoult D. Inhibiting Drp1-mediated mitochondrial fission selectively prevents the release of cytochrome c during apoptosis. *Cell Death Differ*. 2007;14(6):1086–1094.
61. Brown MR, Geddes JW, Sullivan PG. Brain region-specific, age-related, alterations in mitochondrial responses to elevated calcium. *J Bioenerg Biomembr*. 2004;36(4):401–406.
62. Danias J, Lee KC, Zamora MF, et al. Quantitative analysis of retinal ganglion cell (RGC) loss in aging DBA/2NNia glaucomatous mice: comparison with RGC loss in aging C57/BL6 mice. *Invest Ophthalmol Vis Sci*. 2003;44(12):5151–5162.
63. Gross RL, Ji J, Chang P, et al. A mouse model of elevated intraocular pressure: retina and optic nerve findings. *Trans Am Ophthalmol Soc*. 2003;101:163–169.
64. Mabuchi F, Aihara M, Mackey MR, Lindsey JD, Weinreb RN. Optic nerve damage in experimental mouse ocular hypertension. *Invest Ophthalmol Vis Sci*. 2003;44(10):4321–4330.
65. Lindsey JD, Weinreb RN. Elevated intraocular pressure and transgenic applications in the mouse. *J Glaucoma*. 2005;14(4):318–320.
66. Gottlieb E. OPA1 and PARL keep a lid on apoptosis. *Cell*. 2006;126(1):27–29.